RSC Advances

PAPER

View Article Online
View Journal | View Issue

Cite this: *RSC Adv.*, 2017, **7**, 26097

Integrating metallic nanoparticles of Au and Pt with MoS_2–CdS hybrids for high-efficient photocatalytic hydrogen generation *via* plasmon-induced electron and energy transfer†

Kai Chen,‡[ab] Liang Ma,‡[a] Jia-Hong Wang,‡[a] Zi-Qiang Cheng,[a] Da-Jie Yang,[ab] Ying-Ying Li,[a] Si-Jing Ding,*[a] Li Zhou*[a] and Qu-Quan Wang*[ab]

Semiconductor-based photocatalytic H_2 generation is a promising approach to convert solar energy, but single-component photocatalysts still suffer from low efficiency limited by the fast charge recombination. Here, we investigate the high-efficient photocatalytic hydrogen generation of (MoS_2–CdS)/Au and (MoS_2–CdS)/Pt hybrids, and demonstrate the plasmon-induced electron and energy transfer as well as the co-catalytic effect of metallic nanoparticles (NPs). In these hybrids, visible-light-harvester CdS NPs as well as plasmonic Au NPs or co-catalyst Pt NPs were grown on the monolayer MoS_2 nanosheets. The photocatalytic H_2 generation under visible light irradiation of (MoS_2–CdS)/Au and (MoS_2–CdS)/Pt is respectively 3.2 times and 2.4 times that of MoS_2–CdS. Intriguingly, the co-effect of Au NPs and Pt NPs leads to the 17 times enhancement. The plasmonic Au NPs in the hybrids play multiply significant roles to increase efficiency of H_2 generation: (1) enhance light-harvesting and charge separation in the MoS_2–CdS subunit; (2) provide multiply plasmon-mediated hot electron injection channels; (3) amplify the co-catalyst effect of Pt. The present work offers a promising approach for the rational integration of multi-component photocatalyst to improve photocatalytic performance.

Received 6th April 2017
Accepted 10th May 2017

DOI: 10.1039/c7ra03912c

rsc.li/rsc-advances

Introduction

With the rapid development of industry and economy, clean and sustainable energy technologies are urgent for solving energy and environment problems.[1–7] Since the first report of photoelectrochemical water splitting using TiO_2 by Fujishima and Honda, photocatalytic hydrogen generation has attracted intense attention and been regarded as one possible candidate for future energy supply.[8] Numerous semiconductor materials have been applied and developed in this field up to now.[9–15] The valence band (VB) and conduction band (CB) edges of TiO_2 are doable for direct water splitting, while only UV radiation can be utilized due to its wide band gap (E_g = 3–3.3 eV).[8] CdS has attracted much interest arising from its optimal band gap (about 2.4 eV) which is effective for visible-light response and has a suitable conduction band edge for water splitting.[16] However, CdS still suffers from low catalytic efficiency as a result of fast charge carrier recombination and photocorrosion.[16–20]

Multi-component hybrids show obvious advantages over single-component materials due to the synergistic effect among different components.[21–25] Combining light-harvesters with co-catalysts for hydrogen evolution reaction (HER) can promote the photo-excited charge separation and retard the electron–hole recombination. Pt is a typical noble metal co-catalyst, which has the lowest Fermi level among the noble metals and thus possesses the best abilities for trapping electrons and accelerating hydrogen evolution activities.[21,26] Recently, many graphene-like co-catalysts have been applied to incorporate with CdS to construct multi-component nanosystem for high-efficient photocatalytic performance.[23,25] Layered transition-metal dichalcogenide (TMD) nanosheets, such as MS_2 (M = W or Mo), show an excellent performance for the photocatalytic hydrogen evolution as a co-catalyst.[27–29] As a typical layered transition metal sulfide, MoS_2 is shown to be promising as a low cost alternative catalyst to platinum.[30–36] Generally, MoS_2 can be exfoliated to monolayer or few layers by chemical or physical method.[37–39] The mono- or few-layer MoS_2 have negative CB than the H^+/H_2 potential and is suitable for photocatalytic H_2 evolution.[36–39] Hinnemann *et al.* have concluded through density functional calculations that MoS_2 has the free energy

[a]*Key Laboratory of Artificial Micro- and Nano-structures of the Ministry of Education, School of Physics and Technology, Wuhan University, Wuhan 430072, P. R. China. E-mail: qqwang@whu.edu.cn; zhouli@whu.edu.cn; sjding@whu.edu.cn*

[b]*The Institute for Advanced Studies, Wuhan University, Wuhan 430072, P. R. China*

† Electronic supplementary information (ESI) available: TEM images, Fig S1 and S9; extinction spectra, Fig. S4, S5 and S10(a); EDX spectra, Fig. S2; XRD pattern, Fig. S3; photocatalytic H_2 evolution, Fig. S6–S8 and S10(b). See DOI: 10.1039/c7ra03912c

‡ These authors equally contributed to this work.

approach to zero for atomic hydrogen adsorption, close to that of Pt, by the active S atoms on exposed edges.[31–33] Moreover, the 1T-phase MoS_2 nanosheets could offer additional active S atoms as reaction sites for H_2 evolution on their basal plane.[3,5,11] Theoretically, the band gap of MoS_2 could be changed from 1.3 to 1.8 eV corresponding from bulk MoS_2 to monolayer MoS_2.[3,5,32] The MoS_2–CdS multi-component photocatalyst has been shown to exhibit high-efficient photocatalytic activity through suppressing the rapid recombination of charge carriers and accelerating the separation of electron–hole pairs.[40–46] Moreover, integrating two types of co-catalysts including MoS_2 and graphene onto CdS have been reported to further enhance the photocatalytic activity.[47–51]

Loading plasmonic metal NPs can also greatly enhance the photocatalytic activity.[23,52,53] Au nanocrystals are more stable than Ag, which is important in the photocatalytic HER. After combining with semiconductor materials, Au NPs could act as electron trapper to accelerate the charge separation in semiconductor.[17,22,54] Surface plasmon resonance (SPR) of Au nanoparticles induce large local field enhancement, which could improve the light-harvesting ability of semiconductor nearby and then enhance the photocatalytic activity of hybrids.[23–25,53,55] Plasmonic metal NPs could also serve as photo-sensitizers. In this regard, nanostructured Au materials have demonstrated an ability to inject the plasmon-mediated hot electrons into the adjacent semiconductors such as TiO_2, Cu_2O, SnO_2, CdS, *etc.*[25,56–58] Considering the intense light absorption of SPR, the hot electron injection is large beneficial for the photocatalytic performance.[23,53,59] Additionally, the non-radiative energy transfer from the metal plasmonic to the semiconductors could take place *via* near-field interaction,[53,57,60] the large-sized noble metal NPs could act as efficient light-scatters to further improve the light utilization efficiency.[17,53]

Herein, we compared (MoS_2–CdS)/Au and (MoS_2–CdS)/Pt hybrids to demonstrate the high-efficient photocatalytic hydrogen generation. The binary MoS_2–CdS is reported to have efficient photocatalytic activity using MoS_2 as co-catalyst. The monolayer MoS_2 nanosheets also serve as a supporting framework and an electron delivery channel with high mobility.[42] The ternary hybrids of (MoS_2–CdS)/Au and (MoS_2–CdS)/Pt are synthesized for exhibiting the plasmonic enhancement and the co-catalyst effect, respectively. We also integrated the enhancement effects of Au and Pt NPs into one hybrid. The underlying mechanisms of high-efficient photocatalytic hydrogen generation *via* plasmon-induced electron and energy transfer as well as the synergistic effects of each component are discussed.

Experimental

Materials

Chloroauric acid ($HAuCl_4 \cdot 4H_2O$, 99.99%), L-ascorbic acid (AA, 99.7%), cadmium acetate ($Cd(AC)_2$, 99.5%), thioacetamide (TAA, 99%), hexamethylenetetramine (HMT, 99.5%), sodium sulfite (Na_2SO_3, 99.5%), sodium sulfide (Na_2S, 99.5%), methanol, (hydro)chloroplatinic acid (H_2PtCl_6, 99.5%), and sodium citrate ($Na_3C_6H_5O_7 \cdot 2H_2O$, 96%) were purchased from Sinopharm Chemical Reagent Co. Ltd. (Shanghai, China). Hexadecyltrimethylammonium bromide (CTAB, 99.0%) was purchased from Amresco, Inc. (USA). Exfoliated monolayer MoS_2 nanosheets were obtained from Nanjing XFNANO Materials Tech Co., Ltd. All chemicals were used as-received and without further purification. All aqueous solutions were freshly prepared by using double-distilled water.

Synthesis of CdS and MoS_2–CdS nanostructures

CdS NPs were synthesized by mixing 1 mL HMT (0.1 M), AA (0.1 M), CTAB (0.1 M), 80 μL TAA (0.1 M) and 60 μL $Cd(AC)_2$ (0.1 M) with stirring at 90 °C for 3 hours.[61] The final product was centrifuged, washed and re-dispersed in distilled water for further use. For the synthesis of MoS_2–CdS, 2 mL MoS_2 (1 mg mL^{-1}), 1 mL HMT (0.1 M), 1 mL AA (0.1 M) and 1 mL CTAB (0.1 M) were mixed in a glass tube (10 mL). After 80 μL TAA (0.1 M) and 60 μL $Cd(AC)_2$ (0.1 M)were added into the premade aqueous solution, the mixed solution were stirred and heated at 90 °C for 3 hours. The final product was centrifuged, washed and re-dispersed in distilled water for further use.

Synthesis of (MoS_2–CdS)/Au nanostructures

The prepared MoS_2–CdS was dispersed in 20 mL pure water and mixed with 300 μL sodium citrate (10 mM). Then 200 μL $HAuCl_4$ (10 mM) are injected. The mixed solution was kept in room temperature for 1 hour. The final product was centrifuged, washed and re-dispersed in distilled water for further use.[22]

Synthesis of (MoS_2–CdS)/Pt nanostructures

The prepared MoS_2–CdS was dispersed in 20 mL pure water. Then 5 mL methanol and 600 μL H_2PtCl_6 (10 mM) was added with stirring under 300 W Xe light radiation for 0.5 hours.[20,62] The final product was centrifuged, washed and re-dispersed in distilled water for further use.

Synthesis of Pt/MoS_2–CdS/Au nanostructures

The method of preparing quaternary sample was similar with that of (MoS_2–CdS)/Pt except the MoS_2–CdS solution was replaced by the (MoS_2–CdS)/Au solution. The final product was centrifuged, washed and re-dispersed in distilled water for further use.[20,22,62]

Evaluation of photocatalytic activities

The visible-light photocatalytic hydrogen evolution tests were performed in a quartz tube reactor with a rubber septum. In the quartz tube reactor, 50 mg photocatalyst powders were dispersed in 50 mL of aqueous solution containing 0.25 M Na_2SO_3 and 0.35 M Na_2S as sacrificial reagents. The reactor was evacuated by a pump under stirring for 30 min to remove any dissolved air. The light source was a 300 W Xenon lamp equipped with an ultraviolet cut-off filter (λ > 420 nm). The temperature of the suspension was maintained throughout the photocatalytic tests by using an external water cooling system operated at 6 °C, against the temperature rise by the light radiation. The amount of hydrogen gas was automatically analyzed by using online gas chromatography (Tianmei GC-7806).

Characterization

The transmission electron microscope (TEM) and high-resolution TEM (HRTEM) images were obtained with a JEOL 2010 HT and a JEOL 2010 FET, respectively. Energy-dispersive X-ray spectra (EDX) analysis was performed on an energy-dispersive X-ray spectrometer incorporated in the HRTEM. X-Ray diffraction (XRD) patterns were obtained on a Bruker D8 advance X-ray diffractometer with Cu-α irradiation ($\lambda = 0.15418$ nm). The absorption spectra were tested by a UV-Vis-NIR spectrophotometry (Cary 5000, Varian).

Result and discussion

The detail procedures for preparing the (MoS_2–CdS)/Au and (MoS_2–CdS)/Pt hybrids are shown in Fig. 1. Base on monolayer MoS_2 nanosheets, the MoS_2–CdS hybrids are first synthesized through *in situ* growth of CdS onto the MoS_2 nanosheets *via* a facile hydrothermal process using $Cd(AC)_2$ as cadmium source and TAA as sulfur source. The (MoS_2–CdS)/Au hybrids are synthesized by loading Au NPs on the MoS_2–CdS through reducing $HAuCl_4$ by sodium citrate. To obtain the (MoS_2–CdS)/Pt hybrids, Pt NPs are deposited onto the MoS_2–CdS by a photodeposition method with the controlled size and density of Pt (Fig. S1†).

The nanostructure structures of the as-synthesized samples are observed in-depth under TEM. The representative TEM images of MoS_2 monolayer nanosheet, MoS_2–CdS, (MoS_2–CdS)/Au and (MoS_2–CdS)/Pt hybrids are given in Fig. 2(a and d). As shown in Fig. 2(b), the loaded CdS NPs on the monolayer MoS_2 nanosheets have the size no larger than 50 nm. The connection between MoS_2 and CdS is firm owing to the presence of the common S^{2-} anions on the exposed edges of MoS_2.[47] After introducing the plasmonic Au NPs (Fig. 2(c)), the MoS_2 nanosheets are decorated by dispersed Au NPs while some Au NPs show intimate intact with CdS NPs. The Au spherical NPs have the size of 10–30 nm. The existence of Au NPs not only enhances the visible absorption of the nanosystem, but also brings large local field enhancement. Besides, small-sized Pt NPs are photodeposited onto the MoS_2–CdS to form (MoS_2–CdS)/Pt hybrids (Fig. 2(d)).

To further identify and verify the components in the hybrids, we exhibit the HRTEM images of MoS_2, MoS_2–CdS, (MoS_2–CdS)/Au and (MoS_2–CdS)/Pt hybrids. Fig. 3(a) shows that monolayer MoS_2 nanosheets have an obvious lattice spacing of 0.27 nm corresponding to its (100) facet.[37] For the MoS_2–CdS in Fig. 3(b), a clear lattice spacing of 0.33 nm is in agreement with the (002) facet of CdS. As shown in Fig. 3(c), the displayed fringes with lattice spacings of 0.23 nm and 0.33 nm are corresponding to the (111) facet of Au and (002) facet of CdS, respectively.[42–46] The (MoS_2–CdS)/Pt in Fig. 3(d) shows a lattice spacing of 0.22 nm, matching with the (111) facet of Pt.[23] The EDX and XRD patterns in Fig. S2(a) and S3† display the presence of Cd, Mo, S, Au elements for (MoS_2–CdS)/Au.

The optical properties of the as-synthesized samples with same concentrations were studied by the extinction spectra. As shown in Fig. 4 and Fig. S4,† the pure monolayer MoS_2 nanosheets exhibit characteristic absorption band around 400 and

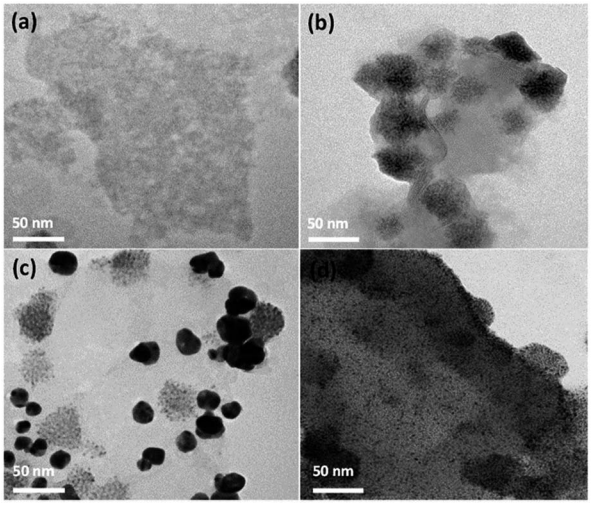

Fig. 2 TEM images of MoS_2 (a), MoS_2–CdS (b), (MoS_2–CdS)/Au (c) and (MoS_2–CdS)/Pt (d) heterostructures.

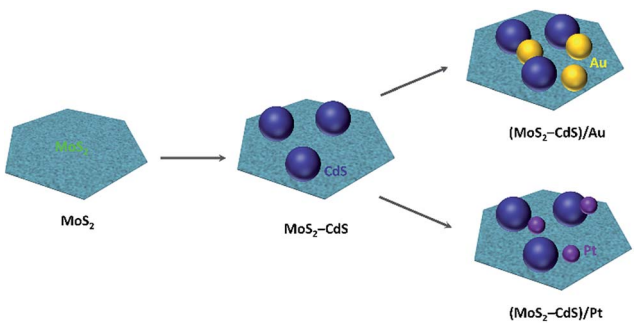

Fig. 1 Schematic illustration of growth mechanism of (MoS_2–CdS)/Au and (MoS_2–CdS)/Pt heterostructures.

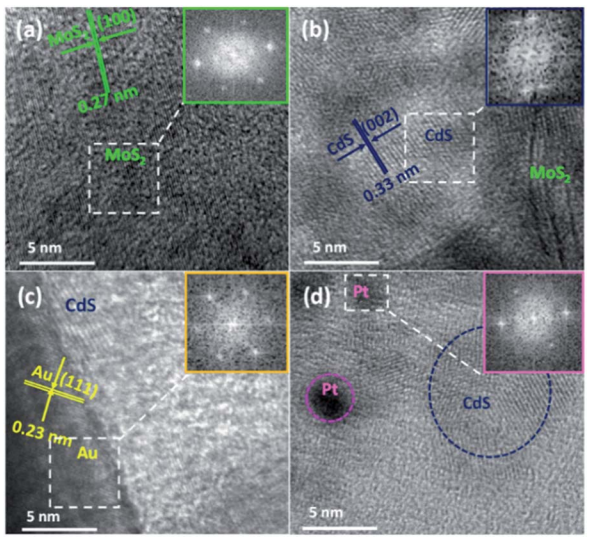

Fig. 3 HRTEM images of MoS_2 (a), MoS_2–CdS (b), (MoS_2–CdS)/Au (c) and (MoS_2–CdS)/Pt (d) heterostructures.

600 nm, the two bands are relative weak. As expected, after the loading of CdS, the MoS_2–CdS hybrids possess the hybrid absorption of MoS_2 and CdS which shows a distinct CdS absorption with an absorption edge at 475 nm. Interestingly, after introducing the Au NPs onto MoS_2–CdS hybrids, the light absorption capability can be further enhanced in visible light. A strong absorption band around 600 nm arises from the SPR of Au NPs.[23,59,63] For (MoS_2–CdS)/Pt, the deposition of Pt NPs on MoS_2–CdS enhances the absorption which will benefit the photocatalytic performance.[18]

The photocatalytic performance for H_2 generation of the prepared CdS, MoS_2–CdS, (MoS_2–CdS)/Au and (MoS_2–CdS)/Pt are compared in Fig. 5. All the H_2 generation reaction are evaluated under a visible light illumination ($\lambda > 420$ nm) by using 50 mL aqueous solution with 0.25 M Na_2SO_3 and 0.35 M Na_2S as an environmentally friendly scavenger to consume holes from the VB of semiconductors and Au NPs.[17,25,55] The average rate of consecutive 3 hours for H_2 generation is recorded to assess the HER photocatalytic performance of the catalysts.

The results plotted in Fig. 5(a) show the amounts of hydrogen steadily increase with the reaction time. The pure CdS shows the lowest photocatalytic activity, while both the MoS_2–CdS, (MoS_2–CdS)/Au and (MoS_2–CdS)/Pt hybrids show enhanced activities. The hydrogen evolution rates of MoS_2–CdS, (MoS_2–CdS)/Au hybrids and (MoS_2–CdS)/Pt are 589, 1878 and 1398 μmol h^{-1} g^{-1}, nearly 15 times, 46 and 34 times that of pure CdS (41 μmol h^{-1} g^{-1}), respectively (Fig. 5(b)). For optimizing the enhanced effect of Au NPs on the photocatalytic H_2 production activities, a series of (MoS_2–CdS)/Au hybrids with different amounts of Au NPs have been prepared (Fig. S5†). Through evaluating the time-dependent photocatalytic H_2 evolution by (MoS_2–CdS)/Au with different quality percentages of Au (Fig. S6†), we found the (MoS_2–CdS)/Au with 6% quality percentage of Au exhibit the highest efficiency of photocatalytic H_2 evolution. A suitable molar ratio of Au in the hybrid nanosystem is important for optimizing the photocatalytic activity,

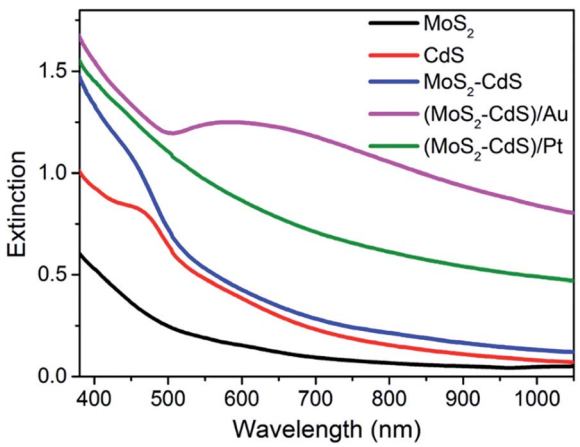

Fig. 4 Extinction spectra of single-layer MoS_2 nanosheets, CdS NPs, MoS_2–CdS, (MoS_2–CdS)/Au and (MoS_2–CdS)/Pt heterostructures.

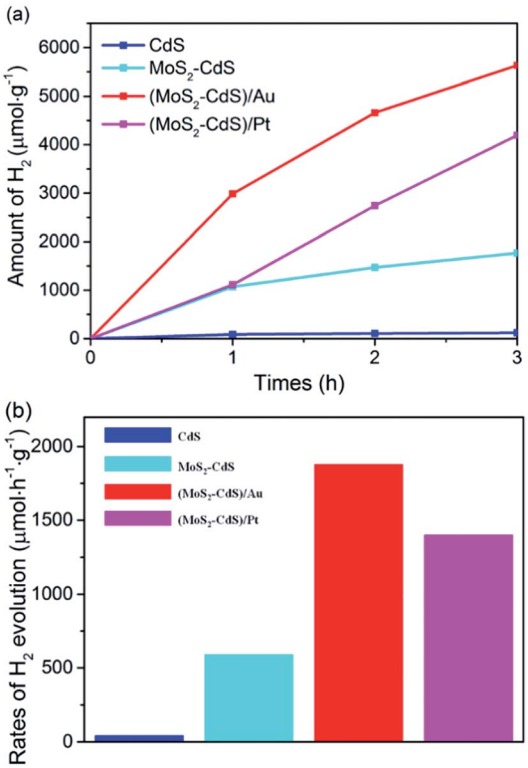

Fig. 5 Photocatalytic activity of the as-synthesized samples for H_2 evolution reaction. Time-dependent photocatalytic H_2 evolution for CdS nanoparticles, MoS_2–CdS, (MoS_2–CdS)/Au and (MoS_2–CdS)/Pt heterostructures (a); comparison of the average H_2 evolution rate in 3 hours under visible light irritation for CdS, MoS_2–CdS, (MoS_2–CdS)/Au and (MoS_2–CdS)/Pt heterostructures (b).

while the excess amount of Au leads to a decrease of H_2 evolution due to the shielding effect.[7,23,26]

The good photocatalytic activity of the MoS_2–CdS subunit is discussed in many literatures.[40–46] CdS is an idea visible light harvester with the band gap of 2.4 eV, matching well with the solar light irradiation.[55] The CB bottom positions of MoS_2 nanosheets and CdS are respectively −0.13 V and −0.35 V (*vs.* NHE).[28,32,42] Under the visible light irradiation of $\lambda \geq 420$ nm, the light absorption induces the electron transition to the CB of CdS. The photo-excited electrons in CdS could easily transfer into the CB of MoS_2 due to the ideal band alignment of MoS_2–CdS, which accelerates charge separation and retard the photo-excited carrier recombination in CdS.[40–46] MoS_2 nanosheets act as electron delivery channels with high mobility.[35,40,42] Owing to the active S atoms for hydrogen adsorption on exposed edges and on the basal plane of 1T-phase MoS_2, the monolayer MoS_2 nanosheets as co-catalysts provide a lot of active sites for the atomic hydrogen adsorption in the HER,[40,42] producing the efficient photocatalytic activity of MoS_2–CdS.

For the (MoS_2–CdS)/Au, the mechanisms of plasmon-induced electron and energy transfer plays a critical role in the photocatalytic activity Fig. 6(a). Firstly, the large field enhancement produced by the SPR of Au NPs could improve the light-harvesting ability and photo-excited carrier concentration of CdS in the vicinity (pathway i). Secondly, the SPR with intense

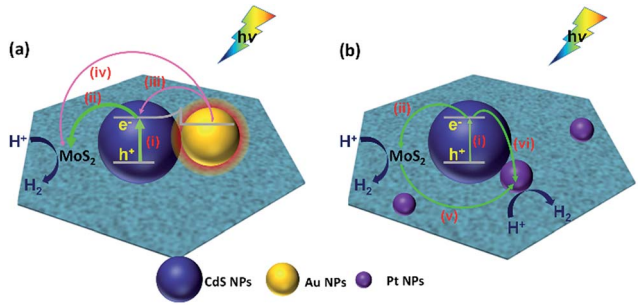

Fig. 6 Schematic illustration of underlying mechanisms *via* plasmon-induced electron and energy transfer as well as the synergistic effects for photocatalytic H_2 evolution reaction using (MoS_2–CdS)/Au (a) and (MoS_2–CdS)/Pt (b) heterostructures.

absorption at 600 nm of Au harvests energy from the light irradiation. The plasmon relaxation produces energetic hot electrons (pathway iii and iv), which could overcome the Schottky barrier of metal–semiconductor interfaces and inject into and MoS_2 (ref. 64 and 65) and CdS,[18,55,58] considering the intimate intact of Au with CdS and Au with MoS_2. Thirdly, the electrons migration from CdS to MoS_2 (pathway ii) can also be improved by the build-in internal electric field at the heterojunction interface.

(MoS_2–CdS)/Pt shows the higher H_2 evolution than MoS_2–CdS due to the excellent co-catalytic effect of Pt NP.[20,21,62] As Fig. 6(b) shown, the electron–hole pairs generation under light irradiation (pathway i) and the photo-excited charge separation (pathway ii) of the MoS_2–CdS subunit has been discussed above. For the ternary (MoS_2–CdS)/Pt, the Pt NPs are distributed on both MoS_2 and CdS. Due to the lower Fermi level and zero-approaching free energy of hydrogen adsorption/desorption, Pt NPs can easily trap the electrons from MoS_2 (pathway v) (ref. 66 and 67) and CdS (pathway vi),[18,20,62] and act as the active sites for the HER. Then the photocatalytic H_2 generation is enhanced by the Pt deposition.

Based on the photocatalytic activity of (MoS_2–CdS)/Au and (MoS_2–CdS)/Pt, we probe and analyze the detailed mechanism between the reaction process using formulation. We describe the aforementioned enhancement mechanisms with the enhancement factors by Au (EF_{Au}) and Pt (EF_{Pt}) as following equations:

$$\begin{aligned} EF_{Au} &= \frac{HER\_rate[(MoS_2 - CdS)/Au]}{HER\_rate[MoS_2 - CdS]} \\ &= \frac{e_P\alpha_{CdS}k_{CdS\rightarrow MoS_2} + \alpha_{Au}(k_{Au\rightarrow CdS}k_{CdS\rightarrow MoS_2} + k_{Au\rightarrow MoS_2})}{\alpha_{CdS}k_{CdS\rightarrow MoS_2}} \\ &= e_P + EF_{Hot\_Sulfide}, \end{aligned} \quad (1)$$

$$\begin{aligned} EF_{Pt} &= \frac{HER\_rate[(MoS_2 - CdS)/Pt]}{HER\_rate[MoS_2 - CdS]} \\ &= \frac{\alpha_{CdS}k_{CdS\rightarrow MoS_2} + \alpha_{CdS}(k_{CdS\rightarrow Pt} + k_{CdS\rightarrow MoS_2}k_{MoS_2\rightarrow Pt})}{\alpha_{CdS}k_{CdS\rightarrow MoS_2}}, \end{aligned} \quad (2)$$

where e_p describes the field enhancement factor of SPR; α_{CdS} and α_{Au} describes the absorption cross-section of CdS and Au, respectively; $k_{CdS\rightarrow MoS_2}$, $k_{Au\rightarrow CdS}$, $k_{Au\rightarrow MoS_2}$, $k_{CdS\rightarrow Pt}$ and $k_{MoS_2\rightarrow Pt}$ describe the electron transfer rate from CdS to MoS_2, Au to CdS, Au to MoS_2, CdS to Pt, and MoS_2 to Pt, respectively. Here, we mainly take into account the efficient HER on MoS_2 and Pt, while ignore the HER on CdS due to the low efficiency. $EF_{Hot\_Sulfide}$ is the enhancement factor by the hot electron injection into the two sulfides (pathway iii and iv shown in Fig. 6(a)).[23,54,68] From the experiment results in Fig. 4 and 5, $EF_{Au} = 3.2$ and $EF_{Pt} = 2.4$ for the ternary hybrids of (MoS_2–CdS)/Au and (MoS_2–CdS)/Pt, respectively.

In order to achieve the high-efficient photocatalytic hydrogen generation, the efficient co-catalytic of Pt and plasmonic Au NPs are further integrated into the multi-component nanosystem. The photocatalytic performance of the Pt/MoS_2–CdS/Au hybrids is evaluated and compared with that of MoS_2–CdS, (MoS_2–CdS)/Pt, and (MoS_2–CdS)/Au (Fig. 7(a)). A suitable molar ratio of Pt/Au in the hybrid nanosystem is important for optimizing the photocatalytic activity. The Pt/MoS_2–CdS/Au hybrids exhibit a largely enhanced photocatalytic performance (10 476 μmol h^{-1} g^{-1}), which is 17 times that of MoS_2–CdS. The photocurrent responses of CdS, MoS_2–CdS, (MoS_2–CdS)/Pt, (MoS_2–CdS)/Au and Pt/MoS_2–CdS/Au samples maintain the trend of the enhancement in the hydrogen generation, and the Pt/MoS_2–CdS/Au achieves the highest photocurrent response among all the samples arising from co-effect of integration of Au and Pt with MoS_2–CdS hybrids contributing to the charge separation. It is not a simple linear superposition of the enhancement factor by Au and Pt. The large enhanced hydrogen evolution rate for the Pt/MoS_2–CdS/Au hybrids is originated from the synergistic effect of each component including the co-catalytic effect of Pt NPs and monolayer MoS_2 along with the significant role of Au NPs, in which the mechanism of plasmon-induced electron and energy transfer is critical important (Fig. S8†).[53] We schematically illustrate the proposed mechanism for photocatalytic H_2 production in Fig. 7(b). These effects are shown in the following equation:

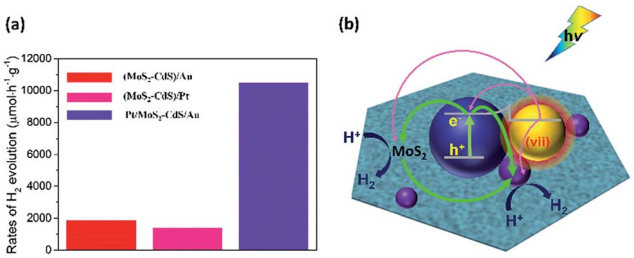

Fig. 7 Photocatalytic H_2 evolution rate under visible light irritation for (MoS_2–CdS)/Au, (MoS_2–CdS)/Pt and Pt/MoS_2–CdS/Au heterostructures (a); schematic illustration of underlying mechanisms *via* plasmon-induced electron and energy transfer as well as the synergistic effects for photocatalytic H_2 evolution reaction using Pt/MoS_2–CdS/Au heterostructures (b).

$$\begin{aligned}EF_{Au+Pt} &= \frac{HER\_rate[Pt/MoS_2 - CdS/Au]}{HER\_rate[MoS_2 - CdS]} \\ &= \frac{e_p\alpha_{CdS}k_{CdS\to MoS_2} + e_p\alpha_{CdS}(k_{CdS\to Pt} + k_{CdS\to MoS_2}k_{MoS_2\to Pt})}{\alpha_{CdS}k_{CdS\to MoS_2}} \\ &+ \frac{\alpha_{Au}(k_{Au\to CdS}k_{CdS\to MoS_2} + k_{Au\to MoS_2})(1 + k_{MoS_2\to Pt}) + \alpha_{Au}k_{Au\to Pt}}{\alpha_{CdS}k_{CdS\to MoS_2}} \\ &= e_pEF_{Pt} + EF_{Hot\_Semi} + EF_{Hot\_Pt} \\ &= EF_{Au} + e_p(EF_{Pt} - 1) + EF_{Hot\_Pt},\end{aligned} \quad (3)$$

where $k_{Au\to Pt}$ describes the rate of a new hot electron channel from Au to Pt.[69,70] EF_{Hot_Pt} is the enhancement factor caused by the hot electron transfer finally to Pt (see detail expression in ESI†).

The eqn (3) indicates that, in the Pt/MoS_2–CdS/Au hybrids, th e co-catalyst effect of Pt NPs is amplified by the plasmonic field enhancement described by e_pEF_{Pt}. In this case, the flows of pathways (i, ii, v and vi) are all greatly enhanced by the plasmonic local field, as the thicker arrows shown in Fig. 7(b). Furthermore, the three hot electron channels (Au to Pt, Au to CdS and Au to MoS_2) contribute the photocatalytic hydrogen generation rate, which are absent in the (MoS_2–CdS)/Pt. Compared with the (MoS_2–CdS)/Au, the amplified Pt co-catalytic effect is involved into the Pt/MoS_2–CdS/Au hybrids, which is very high-efficient for hydrogen generation. Meanwhile, the direct intact between Au and Pt produces a new channel for the plasmon-mediated hot injection effect. With the help of plasmon-induced electron and energy transfer as well as the synergistic effects in the Pt/MoS_2–CdS/Au hybrids, the photocatalytic hydrogen generation rate is dramatically enhanced.

Conclusions

In summary, the (MoS_2–CdS)/Au and (MoS_2–CdS)/Pt hybrids were synthesized for the first time to achieve high-efficient photocatalytic performance for hydrogen generation. Compared with the efficient binary photocatalyst of MoS_2–CdS, the visible-light-driven hydrogen evolution reaction rate of the (MoS_2–CdS)/Au and (MoS_2–CdS)/Pt are enhanced largely. The enhancement factor for (MoS_2–CdS)/Au and (MoS_2–CdS)/Pt are 3.2 times and 2.4 times, which import the plasmonic enhancement effect of Au and the co-catalyst effect of Pt, respectively. Intriguingly, the co-effect of Au NPs and Pt NPs leads to the 17 times enhancement. The construction of multi-component hybrids with metallic nanoparticles of Au and Pt provide a meaningful strategy for pursuing the high-efficient photocatalytic H_2 production.

Acknowledgements

This work was supported by the Natural Science Foundation of China (11374236 and 11674254).

References

1 H. Tada, T. Mitsui, T. Kiyonaga, T. Akita and K. Tanaka, *Nat. Mater.*, 2006, **5**, 782–786.
2 Q. Xiang, J. Yu and M. Jaroniec, *J. Am. Chem. Soc.*, 2012, **134**, 6575–6578.
3 X. Huang, C. Tan, Z. Yin and H. Zhang, *Adv. Mater.*, 2014, **26**, 2185–2204.
4 S. Mubeen, J. Lee, D. Liu, G. D. Stucky and M. Moskovits, *Nano Lett.*, 2015, **15**, 2132–2136.
5 K. Chang, X. Hai and J. Ye, *Adv. Energy Mater.*, 2016, **6**, 1502555.
6 P. Kalisman, Y. Nakibli and L. Amirav, *Nano Lett.*, 2016, **16**, 1776–1781.
7 X. Zong, J. Han, G. Ma, H. Yan, G. Wu and C. Li, *J. Phys. Chem. C*, 2011, **115**, 12202–12208.
8 A. Fujishima, *Nature*, 1972, **238**, 37–38.
9 Q. Li, H. Meng, P. Zhou, Y. Zheng, J. Wang, J. Yu and J. Gong, *ACS Catal.*, 2013, **3**, 882–889.
10 Y. P. Xie, Z. B. Yu, G. Liu, X. L. Ma and H.-M. Cheng, *Energy Environ. Sci.*, 2014, **7**, 1895.
11 H. Du, H. L. Guo, Y. N. Liu, X. Xie, K. Liang, X. Zhou, X. Wang and A. W. Xu, *ACS Appl. Mater. Interfaces*, 2016, **8**, 4023–4030.
12 Y.-J. Yuan, Z.-J. Ye, H.-W. Lu, B. Hu, Y.-H. Li, D.-Q. Chen, J.-S. Zhong, Z.-T. Yu and Z.-G. Zou, *ACS Catal.*, 2016, **6**, 532–541.
13 X. Liu, Z. Xing, Y. Zhang, Z. Li, X. Wu, S. Tan, X. Yu, Q. Zhu and W. Zhou, *Appl. Catal., B*, 2017, **201**, 119–127.
14 N. Qin, J. Xiong, R. Liang, Y. Liu, S. Zhang, Y. Li, Z. Li and L. Wu, *Appl. Catal., B*, 2017, **202**, 374–380.
15 Z. Yue, A. Liu, C. Zhang, J. Huang, M. Zhu, Y. Du and P. Yang, *Appl. Catal., B*, 2017, **201**, 202–210.
16 K. Li, M. Han, R. Chen, S. L. Li, S. L. Xie, C. Mao, X. Bu, X. L. Cao, L. Z. Dong, P. Feng and Y. Q. Lan, *Adv. Mater.*, 2016, **28**, 8906–8911.
17 Q. Zhao, M. Ji, H. Qian, B. Dai, L. Weng, J. Gui, J. Zhang, M. Ouyang and H. Zhu, *Adv. Mater.*, 2014, **26**, 1387–1392.
18 L. Ma, K. Chen, F. Nan, J.-H. Wang, D.-J. Yang, L. Zhou and Q.-Q. Wang, *Adv. Funct. Mater.*, 2016, **26**, 6076–6083.
19 M. Luo, W. Yao, C. Huang, Q. Wu and Q. Xu, *J. Mater. Chem. A*, 2015, **3**, 13884–13891.
20 L. Shang, B. Tong, H. Yu, G. I. N. Waterhouse, C. Zhou, Y. Zhao, M. Tahir, L.-Z. Wu, C.-H. Tung and T. Zhang, *Adv. Energy Mater.*, 2016, **6**, 1501241.
21 A. Litke, T. Weber, J. P. Hofmann and E. J. M. Hensen, *Appl. Catal., B*, 2016, **198**, 16–24.
22 J. Cai, X. Wu, S. Li and F. Zheng, *Appl. Catal., B*, 2017, **201**, 12–21.
23 Z. Zhang, Y. Huang, K. Liu, L. Guo, Q. Yuan and B. Dong, *Adv. Mater.*, 2015, **27**, 5906–5914.
24 J. Zhang, X. Jin, P. I. Morales-Guzman, X. Yu, H. Liu, H. Zhang, L. Razzari and J. P. Claverie, *ACS Nano*, 2016, **10**, 4496–4503.
25 A. Zada, M. Humayun, F. Raziq, X. Zhang, Y. Qu, L. Bai, C. Qin, L. Jing and H. Fu, *Adv. Energy Mater.*, 2016, **6**, 1601190.
26 H. Li, H. Yu, L. Sun, J. Zhai and X. Han, *Nanoscale*, 2015, **7**, 1610–1615.
27 J. He, L. Chen, Z.-Q. Yi, C.-T. Au and S.-F. Yin, *Ind. Eng. Chem. Res.*, 2016, **55**, 8327–8333.

28 J. Chen, X. J. Wu, L. Yin, B. Li, X. Hong, Z. Fan, B. Chen, C. Xue and H. Zhang, *Angew. Chem., Int. Ed.*, 2015, **54**, 1210–1214.
29 Y. Zhong, G. Zhao, F. Ma, Y. Wu and X. Hao, *Appl. Catal., B*, 2016, **199**, 466–472.
30 H. Li, C. Tsai, A. L. Koh, L. Cai, A. W. Contryman, A. H. Fragapane, J. Zhao, H. S. Han, H. C. Manoharan, F. Abild-Pedersen, J. K. Norskov and X. Zheng, *Nat. Mater.*, 2016, **15**, 364.
31 B. Hinnemann, P. G. Moses, J. Bonde, K. P. Jorgensen, J. H. Nielsen, S. Horch, I. Chorkendorff and J. K. Norskov, *J. Am. Chem. Soc.*, 2005, **127**, 5308–5309.
32 K. Chang, M. Li, T. Wang, S. Ouyang, P. Li, L. Liu and J. Ye, *Adv. Energy Mater.*, 2015, **5**, 1402279.
33 H. He, J. Lin, W. Fu, X. Wang, H. Wang, Q. Zeng, Q. Gu, Y. Li, C. Yan, B. K. Tay, C. Xue, X. Hu, S. T. Pantelides, W. Zhou and Z. Liu, *Adv. Energy Mater.*, 2016, **6**, 1600464.
34 G. Eda, H. Yamaguchi, D. Voiry, T. Fujita, M. Chen and M. Chhowalla, *Nano Lett.*, 2011, **11**, 5111–5116.
35 M. A. Lukowski, A. S. Daniel, F. Meng, A. Forticaux, L. Li and S. Jin, *J. Am. Chem. Soc.*, 2013, **135**, 10274–10277.
36 D. Voiry, M. Salehi, R. Silva, T. Fujita, M. Chen, T. Asefa, V. B. Shenoy, G. Eda and M. Chhowalla, *Nano Lett.*, 2013, **13**, 6222–6227.
37 X. Huang, Z. Zeng, S. Bao, M. Wang, X. Qi, Z. Fan and H. Zhang, *Nat. Commun.*, 2013, **4**, 1444.
38 L. Yuwen, F. Xu, B. Xue, Z. Luo, Q. Zhang, B. Bao, S. Su, L. Weng, W. Huang and L. Wang, *Nanoscale*, 2014, **6**, 5762–5769.
39 G. Ye, Y. Gong, J. Lin, B. Li, Y. He, S. T. Pantelides, W. Zhou, R. Vajtai and P. M. Ajayan, *Nano Lett.*, 2016, **16**, 1097–1103.
40 J. Xiong, Y. Liu, D. Wang, S. Liang, W. Wu and L. Wu, *J. Mater. Chem. A*, 2015, **3**, 12631–12635.
41 J. He, L. Chen, F. Wang, Y. Liu, P. Chen, C. T. Au and S. F. Yin, *ChemSusChem*, 2016, **9**, 624–630.
42 F. Ma, Y. Wu, Y. Shao, Y. Zhong, J. Lv and X. Hao, *Nano Energy*, 2016, **27**, 466–474.
43 X. L. Yin, L. L. Li, W. J. Jiang, Y. Zhang, X. Zhang, L. J. Wan and J. S. Hu, *ACS Appl. Mater. Interfaces*, 2016, **8**, 15258–15266.
44 X.-L. Yin, G.-Y. He, B. Sun, W.-J. Jiang, D.-J. Xue, A.-D. Xia, L.-J. Wan and J.-S. Hu, *Nano Energy*, 2016, **28**, 319–329.
45 K. Zhang, J. K. Kim, M. Ma, S. Y. Yim, C.-L. Lee, H. Shin and J. H. Park, *Adv. Funct. Mater.*, 2016, **26**, 4527–4534.
46 B. Han, S. Liu, N. Zhang, Y.-J. Xu and Z.-R. Tang, *Appl. Catal., B*, 2017, **202**, 298–304.
47 K. Chang, Z. Mei, T. Wang, Q. Kang, S. Ouyang and J. Ye, *ACS Nano*, 2014, **8**, 7078–7087.
48 T. Jia, A. Kolpin, C. Ma, R. C. Chan, W. M. Kwok and S. C. Tsang, *Chem. Commun.*, 2014, **50**, 1185–1188.
49 M. Liu, F. Li, Z. Sun, L. Ma, L. Xu and Y. Wang, *Chem. Commun.*, 2014, **50**, 11004–11007.
50 D. Lang, T. Shen and Q. Xiang, *ChemCatChem*, 2015, **7**, 943–951.
51 M.-Q. Yang, C. Han and Y.-J. Xu, *J. Phys. Chem. C*, 2015, **119**, 27234–27246.
52 H. Wang, T. You, W. Shi, J. Li and L. Guo, *J. Phys. Chem. C*, 2012, **116**, 6490–6494.
53 X.-C. Ma, Y. Dai, L. Yu and B.-B. Huang, *Light: Sci. Appl.*, 2016, **5**, e16017.
54 Y. Ben-Shahar, F. Scotognella, I. Kriegel, L. Moretti, G. Cerullo, E. Rabani and U. Banin, *Nat. Commun.*, 2016, **7**, 10413.
55 X. Ma, K. Zhao, H. Tang, Y. Chen, C. Lu, W. Liu, Y. Gao, H. Zhao and Z. Tang, *Small*, 2014, **10**, 4664–4670.
56 B. Wu, D. Liu, S. Mubeen, T. T. Chuong, M. Moskovits and G. D. Stucky, *J. Am. Chem. Soc.*, 2016, **138**, 1114–1117.
57 S. K. Cushing, J. Li, F. Meng, T. R. Senty, S. Suri, M. Zhi, M. Li, A. D. Bristow and N. Wu, *J. Am. Chem. Soc.*, 2012, **134**, 15033–15041.
58 K. Wu, W. E. Rodriguez-Cordoba, Y. Yang and T. Lian, *Nano Lett.*, 2013, **13**, 5255–5263.
59 M. Kim, Y. K. Kim, S. K. Lim, S. Kim and S.-I. In, *Appl. Catal., B*, 2015, **166–167**, 423–431.
60 F. Nan, S. J. Ding, L. Ma, Z. Q. Cheng, Y. T. Zhong, Y. F. Zhang, Y. H. Qiu, X. Li, L. Zhou and Q. Q. Wang, *Nanoscale*, 2016, **8**, 15071–15078.
61 L. Ma, S. Liang, X.-L. Liu, D.-J. Yang, L. Zhou and Q.-Q. Wang, *Adv. Funct. Mater.*, 2015, **25**, 898–904.
62 Y. Zhu, Z. Chen, T. Gao, Q. Huang, F. Niu, L. Qin, P. Tang, Y. Huang, Z. Sha and Y. Wang, *Appl. Catal., B*, 2015, **163**, 16–22.
63 J. Li, S. K. Cushing, P. Zheng, T. Senty, F. Meng, A. D. Bristow, A. Manivannan and N. Wu, *J. Am. Chem. Soc.*, 2014, **136**, 8438–8449.
64 Y. Shi, J. Wang, C. Wang, T. T. Zhai, W. J. Bao, J. J. Xu, X. H. Xia and H. Y. Chen, *J. Am. Chem. Soc.*, 2015, **137**, 7365–7370.
65 Y. Yu, Z. Ji, S. Zu, B. Du, Y. Kang, Z. Li, Z. Zhou, K. Shi and Z. Fang, *Adv. Funct. Mater.*, 2016, **26**, 6394–6401.
66 X. Li, L. Zhang, X. Zang, X. Li and H. Zhu, *ACS Appl. Mater. Interfaces*, 2016, **8**, 10866–10873.
67 S. Walia, S. Balendhran, Y. Wang, R. Ab Kadir, A. Sabirin Zoolfakar, P. Atkin, J. Zhen Ou, S. Sriram, K. Kalantar-zadeh and M. Bhaskaran, *Appl. Phys. Lett.*, 2013, **103**, 232105.
68 L. Weng, H. Zhang, A. O. Govorov and M. Ouyang, *Nat. Commun.*, 2014, **5**, 4792.
69 Z. Zheng, T. Tachikawa and T. Majima, *J. Am. Chem. Soc.*, 2014, **136**, 6870–6873.
70 Z. Lou, M. Fujitsuka and T. Majima, *ACS Nano*, 2016, **10**, 6299–6305.